

Accepted Manuscript

Title: Structural characteristics and catalytic performance of nanostructured Mn-doped CeO₂ solid solutions towards oxidation of benzylamine by molecular O₂

Author: Agolu Rangaswamy Perala Venkataswamy Damma Devaiah Singuru Ramana Benjaram M. Reddy



PII: S0025-5408(16)32614-9
DOI: <http://dx.doi.org/doi:10.1016/j.materresbull.2016.12.028>
Reference: MRB 9070

To appear in: *MRB*

Received date: 30-8-2016
Revised date: 22-11-2016
Accepted date: 22-12-2016

Please cite this article as: Agolu Rangaswamy, Perala Venkataswamy, Damma Devaiah, Singuru Ramana, Benjaram M.Reddy, Structural characteristics and catalytic performance of nanostructured Mn-doped CeO₂ solid solutions towards oxidation of benzylamine by molecular O₂, Materials Research Bulletin <http://dx.doi.org/10.1016/j.materresbull.2016.12.028>

This is a PDF file of an unedited manuscript that has been accepted for publication. As a service to our customers we are providing this early version of the manuscript. The manuscript will undergo copyediting, typesetting, and review of the resulting proof before it is published in its final form. Please note that during the production process errors may be discovered which could affect the content, and all legal disclaimers that apply to the journal pertain.

Structural characteristics and catalytic performance of nanostructured Mn-doped CeO₂ solid solutions towards oxidation of benzylamine by molecular O₂

Agolu Rangaswamy^{a,b}, Perala Venkataswamy^{a,c}, Damma Devaiah^{a,d}, Singuru Ramana^{a,b}, Benjaram M. Reddy^{a,b,*}

^aInorganic and Physical Chemistry Division, CSIR – Indian Institute of Chemical Technology Uppal Road, Hyderabad – 500 007, India

^bAcademy of Scientific and Innovative Research, CSIR-IICT, India

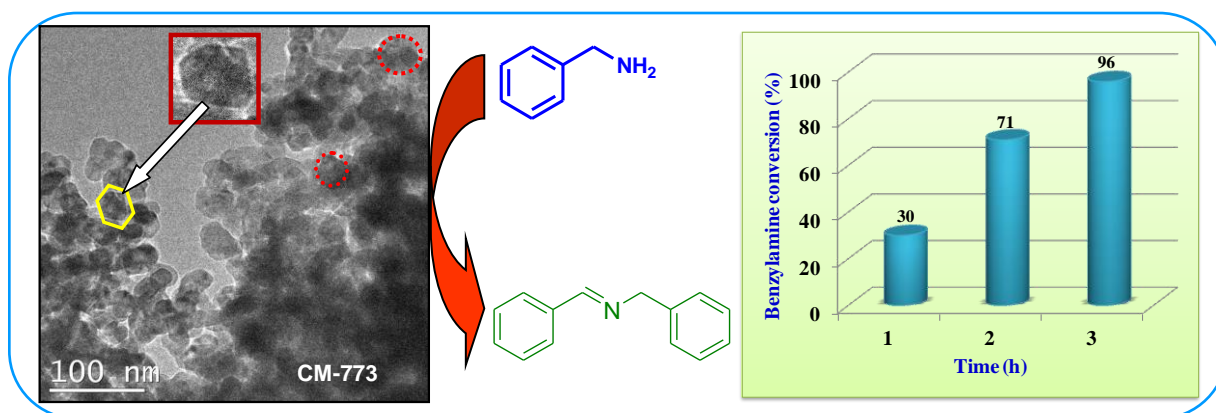
^cDepartment of Chemistry, Osmania University, Hyderabad - 500 007, India

^dChemical Engineering Program, Biomedical, Chemical, and Environmental Engineering, University of Cincinnati, Cincinnati, OH 45221-0012, USA

* Corresponding Author: Tel: +91 40 2719 3510; Fax: +91 40 2716 0921.

E-mail addresses: bmreddy@iict.res.in; mreddyb@yahoo.com

Graphical Abstract



Research Highlights:

- Nanosized Mn-doped ceria solid solutions were synthesized by an economical method.
- Synthesized catalysts were explored for benzylamine oxidation.
- Mn-doped ceria is more active than ceria and MnO_x for benzylamine oxidation.
- The dopant induced structural changes were deeply discussed.
- Mn-doped ceria shows superior catalytic activity towards benzylamine oxidation.

ABSTRACT

This work reports a thorough investigation of nanosized Mn-doped ceria ($\text{Ce}_{0.7}\text{Mn}_{0.3}\text{O}_{2-\delta}$, CM) as an efficient catalyst for oxidation of benzylamine under solvent-free conditions. These catalysts were prepared by a coprecipitation method followed by calcination at 773 and 1073 K. Effect of Mn doping was examined by a variety of characterization techniques. XRD

results confirmed formation of single-phase Ce-O-Mn solid solution, and TEM studies showed nanosized nature of particles. BET surface area of CeO₂ was significantly enhanced after Mn incorporation. Raman, XPS and H₂-TPR results revealed that Mn cations in ceria lattice increase concentration of structural oxygen vacancies and reducibility of ceria. Among various catalysts, the CM calcined at 773 K exhibited a high conversion (~71%), product selectivity (~99.8%), and excellent stability. The better performance has been proved to be due to synergetic interaction between Ce and Mn ions thereby enhanced surface area, improved reducibility, and increased surface adsorbed oxygen species.

KEYWORDS: A. Nanostructures; A. Oxides; C. X-ray diffraction; C. Raman spectroscopy; D. Catalytic properties.

1 Introduction

The selective oxidation of amines to imines has been greatly attracted due to the versatile applications of imines in the organic synthesis [1, 2]. For example, imines are the key building blocks for the synthesis of nitrogen-heterocycles, fine chemicals, α -amino acids, α -amino alcohols, fragrances, fungicides, pharmaceuticals, and agricultural chemicals [3–6]. Additionally, imines are important intermediates in a number of organic reactions, such as addition, reduction, aziridination, β -lactamization, cyclization, condensations, and aza-Diels–Alder reactions [7]. Significant development has been made in recent years in the synthesis of imines, including direct synthesis of imines from amines, condensation of alcohols with amines, self-condensation of amines with oxidants and secondary amines oxidation [8]. Most of these reactions are achieved in solvent media which is conceivably the most active area for green chemistry research. However, solvents have often accounted for the vast majority of mass wasted in syntheses and processes. On the other hand, selective oxidation reactions are performed with stoichiometric amounts of high valent inorganic oxidants, such as chromate or permanganate, as well as with organic oxidants, like 2-iodoxybenzoic acid and N-tert-butylphenylsulfinimidoylchloride [9–12]. Alternatively, researchers have focused on the development of catalytic systems for the selective oxidation of amines into the corresponding imines with green and atom-efficient oxidants, such as O₂ and H₂O₂ [13]. Nevertheless,

achieving sufficient space time-yield with these more sustainable oxidants, while maintaining high levels of selectivity, remains a challenge. The selective oxidation of amines has been studied over a wide variety of heterogeneous catalysts based on noble metals. Despite the excellent catalytic performance of noble metal-based catalysts, their high price due to the limited resources and sensitivity to oxygen poisoning make their applications practically and environmentally unfavourable. Therefore, the development of non-noble metal catalysts and adequate catalytic oxidation performance is of crucial importance from both practical and economical points of view [7, 14–17].

Recently, it has been reported that metal oxide based catalysts could be possible alternatives for selective oxidation of amines [18]. Among the various oxide catalysts, particular attention has been paid to CeO_2 containing systems due to their unique physicochemical properties, linked to high oxygen storage-release capacities via $\text{Ce}^{4+}/\text{Ce}^{3+}$ redox cycles [19]. In this regard, several CeO_2 -based catalysts were tested for oxidation of benzylamines in earlier reports [16, 20]. An enhanced catalytic performance was observed over the CeO_2 -based mixed oxides compared to the individual counterparts, which was ascribed to better redox properties through synergistic interactions between the metal ions [21, 22]. The high specific surface area, large amounts of oxygen vacancy defects and abundant acid properties are found to be the key factors for the observed catalytic efficiency of ceria-based catalysts [23–26].

In addition to CeO_2 -based catalysts, manganese-based oxides have also received considerable attention in heterogeneous catalysis due to their high specific capacitance ready availability of variable oxidation states, better redox properties, environmental compatibility, low cost, and non-toxic nature [27–30]. The doping of metal oxide (e.g., MnO_x) into the CeO_2 is one of the promising ways to modify its physicochemical properties [31, 32]. CeO_2 - MnO_x mixed oxide displays smaller particle size, higher specific surface area, and more number of oxygen vacancies compared with bare ceria, which is ascribed to the co-operation effect of the cerium and dopant [31, 33–35]. Particularly, oxygen vacancies play an important role in the adsorption and activation of gaseous phase oxygen in order to cooperate with the reactant molecules in the oxidation reactions [36]. Therefore, doping of nanoscale manganese oxide into ceria lattice may lead to unusual properties and exceptional catalytic activities.

In accordance with the above aspects, the present work aims at systematically exploring the catalytic oxidation of benzylamine under eco-friendly reaction conditions over CeO_2 - MnO_x mixed oxides prepared by a simple coprecipitation method. The Ce/Mn mole ratio was

optimized and the effect of calcination temperature on the physicochemical properties and catalytic performance was thoroughly investigated. Several characterization techniques such as X-ray diffraction (XRD), inductively coupled plasma-optical emission spectroscopy (ICP-OES), Brunauer–Emmett–Teller (BET) surface area, field emission scanning electron microscope-energy dispersive X-ray analysis (FESEM-EDX), transmission electron microscopy (TEM), high-resolution transmission electron microscopy (HRTEM), Raman spectroscopy (RS), X-ray photoelectron spectroscopy (XPS), temperature-programmed reduction by hydrogen (H_2 -TPR), and temperature-programmed desorption by ammonia (NH_3 -TPD) were employed to understand the effect of the MnO_x doping on the physicochemical properties of the prepared samples and its impact on benzylamine oxidation activity.

2. Experimental Section

2.1 Catalyst Preparation

All of the chemicals used in this study were of analytical grade and used without further purification. The optimized nanostructured $\text{Ce}_{0.7}\text{Mn}_{0.3}\text{O}_{2-\delta}$ (CM, 7:3 mole ratio based on oxides) oxide was prepared by a coprecipitation method through hydrolysis of metal nitrates as precursors. In a typical procedure, appropriate amounts of $\text{Ce}(\text{NO}_3)_2 \cdot 6\text{H}_2\text{O}$ (Aldrich, AR grade, > 99.9%) and $\text{Mn}(\text{NO}_3)_2 \cdot 4\text{H}_2\text{O}$ (Wako Pure Chemical, > 99.9%) were dissolved separately in de-ionized water and mixed together with stirring to form a homogeneous solution. Then the mixed solution was precipitated by drop-wise addition of aqueous ammonia solution (NH_4OH) over a period until the solution pH reached ~9. After room temperature aging for 24 h, the resulting pale brown colored Ce-Mn was decanted, filtered and washed several times with distilled water until free from anion impurities. In this method, Ce and Mn ions in the synthetic solutions were completely precipitated by hydrolysis with aq. ammonia, and therefore, the bulk molar ratio of Ce to Mn was consistent with those of the metal nitrate precursors used in the preparation procedure. The composition of the mixed oxides was confirmed by ICP-OES. The obtained precipitate was oven dried at 373 K for 5 h and ground in an agate mortar. The dried powders were calcined at 773 K for 5 h at a heating rate of 5 K min^{-1} under dry air. Finally, some portions of the finished catalyst were further calcined at 1073 K for 5 h under dry air using the same heating rate to monitor thermal stability. For comparison, the nanocrystalline single oxides, CeO_2 and MnO_x , were also prepared by the same way and calcined at 773 K for 5 h. For convenient purpose, the as-

prepared Mn-doped CeO₂ catalysts calcined at 773 and 1073 K were represented as CM-773 and CM-1073, respectively.

2.2 Catalysts Characterization

XRD patterns were acquired on an X'pert Pro MPD powder diffractometer (PANalytical Company) equipped with a nickel-filtered Cu K α (0.15418 nm) radiation source and a scintillation counter detector (SCD). The scattered intensity data were collected from 2 θ of 2 to 80° by scanning at 0.01° steps with a counting time of 1 s at each step. Crystalline phases were identified by matching with the International Centre for Diffraction Data Powder Diffraction File (ICDD-PDF). The average crystallite size (D) of the samples was determined with the help of Scherrer equation from line broadening and the lattice parameters (a) were estimated through the formulae $a = (h^2 + k^2 + l^2)^{1/2} * (\lambda / 2 \sin \theta)$ using the intensity of the most prominent peak (111).

The elemental analysis was performed by ICP-OES to estimate the respective concentrations of Ce and Mn. For ICP analysis, approximately 50 mg of the sample was dissolved in a solution of 25 ml aqua regia and 475 ml distilled water. Then 10 ml of the above solution was diluted to 250 ml. The measurements were performed on a Thermo Jarrel Ash model IRIS Intrepid II XDL, USA.

The surface area and pore size distribution of the as-prepared samples were determined by N₂ adsorption-desorption isotherms at liquid N₂ temperature (77 K) on a Micromeritics (ASAP 2000) analyzer. Specific surface area and pore size distribution were calculated by BET and Barrett-Joyner-Halenda (BJH) methods, respectively. Prior to the measurements, the samples were pre-treated in a vacuum oven at 473 K for 2 h to remove any residual moisture.

FESEM studies were performed by using a (FESEM, JEOL-7610F) electron microscope to examine surface morphology, and the energy dispersive X-ray analysis (EDX) was used to determine the elemental composition of samples with OXFORD Inca detector interfaced at 5 kV.

The TEM-HRTEM studies were made on a TECNAIG2 TEM microscope equipped with a slow-scan CCD camera and at an accelerating voltage of 200 kV. Samples for TEM analysis were prepared by crushing the materials in an agate mortar and dispersing ultrasonically in ethyl alcohol. After well dispersion, a droplet was deposited on a copper grid

supporting a perforated carbon film and allowed to dry. The specimen was examined under vacuum at room temperature.

Raman spectra were obtained at room temperature on a Horiba Jobin-Yvon HR 800 Raman spectrometer fitted with a confocal microscope and liquid-nitrogen cooled charge-coupled device (CCD) detector. The line at 632 nm of Ar⁺ ion (Spectra Physics) laser was used as an excitation source for the visible Raman spectroscopy. The laser was focused on the sample under a microscope with the diameter of the analyzed spot being ~1 μm . The acquisition time was adjusted according to the intensity of Raman scattering. The wavenumber values reported from the spectra are accurate to within 2 cm^{-1} .

XPS analyses were performed using a PHI 5000 Versa probe (Ulvac-PHI) Spectrometer. The X-ray source utilized was the Mg K α (1253.6 eV) radiation. The analysis was done at room temperature and the pressures were typically in the order of less than 10^{-8} Pa. The charging of samples was corrected by setting the binding energy of the adventitious carbon (C 1s) at 284.5 eV. The samples were out gassed overnight in a vacuum oven at 283 K before XPS measurements. All binding energies were measured within a precision of ± 0.3 eV.

H₂-TPR analysis was used for evaluating the reduction properties of prepared catalysts using an automated Micromeritics AutoChem II-2720 instrument equipped with a thermal conductivity detector (TCD). Approximately 30 mg of the sample mass was placed on top of quartz wool in a U-shaped quartz reactor (Inner diameter 5 mm). The sample was pre-treated at a rate of 10 K min⁻¹ to 473 K under a pure He atmosphere at a flow rate of 30 mL min⁻¹ for 30 min to clean the surface of the catalysts before TPR investigation. After cooling down to room temperature, introducing the reduction agent of 5 vol% H₂/Ar with a flow rate of 20 mL min⁻¹, the temperature was programmatically raised to 1073 K at a ramp of 5 K min⁻¹, keeping all the parameters unchanged. The outlet of the reactor was connected to a cold trap to absorb the water molecules resulted by the reduction of the catalysts.

NH₃-TPD data were collected on a Micromeritics Autochem 2910 Automated Catalyst Characterization System. Each sample (ca. 100 mg) was initially pretreated through heating at 473 K in an ultrahigh pure He stream (30 mL min⁻¹) with a 2 h hold. After that, the furnace temperature was lowered to 373 K, and the samples were then saturated with anhydrous NH₃ (4% in He) at a flow rate of 30 mL min⁻¹ for 1 h. The sample was flushed with 30 mL/min of He for 2 h to remove weakly bound (physisorbed) NH₃, after which the sample temperature

was reduced to 323 K. Once a stable baseline by thermal conductivity detector had been achieved, the temperature was then ramped from 323 K at a rate of 5 °C/min to 973 K.

2.3 Catalytic Activity

The catalytic performance of the prepared samples was investigated for the oxidation of benzylamine using an O₂ balloon under solvent-free conditions. In a typical experiment, 0.2 mmol of substrate and 100 mg of catalyst were taken into a 10 mL round bottom flask and stirred magnetically at required temperature for appropriate time. After completion of the reaction, the catalyst was separated from reaction mixture by centrifugation. The products were confirmed by GC-MS equipped with a DB-5 capillary column and a flame ionization detector (FID). Samples were taken periodically during the reaction and analyzed by GC equipped with BP-20 (wax) capillary column and a FID.

3 Results and Discussion

3.1 Characterization Studies

The synthesized samples were analyzed by powder XRD in order to know the phase purity. An exemplary diffraction pattern of manganese doped ceria catalysts calcined at 773 and 1073 K are provided in Fig. 1. The diffraction patterns of CeO₂ and MnO_x samples calcined at 773 K are also presented for comparison purpose. The pure MnO_x exhibited the diffraction patterns related to mixed phases of Mn₂O₃ (JCDs 41-1442) and Mn₃O₄ (PDF no. 24-0734) without any impurity (as “α” and “β” marked in Fig. 1) [37]. Whereas, the pure ceria and both the manganese doped ceria catalysts exhibit characteristic diffraction peaks of typical cubic fluorite phase of ceria (JCPDS, No. 34-0394) [38]. Evidently, the absence of diffraction peaks pertaining to manganese oxides, namely, MnO₂, Mn₂O₃, and MnO indicates either all the Mn ions have entered into the cubic ceria crystal forming solid solution or else the manganese oxides are present in well dispersed state, which is beyond the instrument's detection limit [31, 39]. Moreover, it can be noted that the diffraction peaks of CM-773 sample are slightly shifted to higher Bragg angles, which can be related to a more significant change of Ce-O environment by strong interaction with the adjacent MnO_x under low calcination conditions. The peak shift can be attributed to the fact that doping of smaller size Mn^{x+} (Mn²⁺ = 0.083 nm; Mn³⁺ = 0.065 nm; Mn⁴⁺ = 0.053 nm) ions leads to contraction of the ceria lattice as reported earlier [40]. Thus, lattice parameter of CM-773 exhibits a smaller value compared to pure ceria (Table 1). The observed key features, such as peak shift, variation in the lattice parameter and absence of XRD peaks pertaining to the dopant metal

oxides evidently confirm the formation of Ce-O-Mn solid solution in CM-773 catalyst. The formation of Ce-O-Mn solid solution led to structural distortions in CeO_2 , which may facilitate the formation of oxygen vacancies in the cubic lattice of ceria [41]. Compared with the pure CeO_2 , the typical diffraction peaks of CM-773 catalyst are broadened and their intensity is also basically decreased, demonstrating that the Ce-Mn mixed oxide has a much smaller crystal size. Following the Scherrer equation, the crystallite size of as-prepared catalysts are calculated by using the full width at half maximum of (111) line of cubic ceria lattice and the results are summarized in Table 1. As expected, the crystallite size of CM-773 was 7.19 nm, which was smaller than other samples especially the single oxides (8.92 nm for CeO_2 and 32.4 nm for MnO_x). For CM-1073 sample, peaks for not only cerium oxide but also Mn oxide were observed (at $2\theta = 55.6^\circ$ corresponding to (440) plane of anatase Mn_2O_3), which might be due to manganese oxide phase (i.e., Mn_2O_3) segregation at elevated thermal treatments. This phenomenon indicates that the interaction between the two kinds of metal oxides got weakened. Moreover, the peaks for CeO_2 became sharper with increasing calcination temperature due to improved crystallinity which in turn resulted in crystallite growth. The chemical compositions of Ce and Mn in CM-773 and CM-1073 are calculated by ICP-OES analysis. The extracted data are reported in Table S1. It is found that the measured Ce and Mn concentrations are in good agreement with the nominal values. The small difference observed may be due to inaccuracies in the preparation of the solution of samples for ICP-OES analysis.

Fig. S1 shows the N_2 adsorption/desorption isotherms of the CeO_2 and MnO_x calcined at 773 K and Mn-doped ceria catalysts calcined at 773 and 1073 K. It can be noted that the profile of the adsorption isotherms of all the samples is type IV according to the IUPAC classification, demonstrating mesoporous character with a small pore size and good homogeneity [42-43]. The formation of mesopores may provide more inner surface areas and active sites for better contact between reactant and adsorbent. According to the P/P_0 position of reflection points shown in Fig. S1, the pore diameters were in the mesopore range. Further, according to the IUPAC classification, the hysteresis of samples can be developed in the multilayer range of physisorption isotherms and thus the hysteresis can be classified as H3 type. This type of hysteresis confirms the formation of non-uniform slit shaped pores through the aggregation of the plate-like particles. Moreover, in case of Mn-doped ceria catalyst with increasing calcination temperature from 773 to 1073 K, the hysteresis loop shifted to a higher relative pressure (P/P_0) range and the area of the hysteresis loops gradually became smaller.

It is generally accepted that the shift of the hysteresis loop to higher relative pressures indicates the presence of larger pore diameters (Table 1). This is confirmed by the pore size distribution (PSD) curves that were obtained from the desorption isotherms (Fig. S1 insets). A quite narrow and unimodal pore size distribution was obtained for all the samples. The figure also confirms that with increasing calcination temperature, the pore size increases, accompanied by decrease in the surface areas as a result of pore destruction and particle sintering. The textural properties including BET surface area, total pore volume and average pore diameter of the samples studied in the present investigation are summarized in Table 1. The surface areas of pure ceria and manganese oxide were found to be 41 and 28 m² g⁻¹, respectively, which were less than that for the manganese incorporated ceria nanoparticles, in particular with CM-773 (Table 1). The increase in the surface area of CM-773 may be due to incorporation of Mn^{x+} into its lattice thereby inhibits crystalline growth of ceria and this result is well matched with the XRD results [44]. It is well-known that the porous nanostructured materials with a high surface area are suitable for catalytic oxidation reactions, due to the high number of catalytically active centers per unit mass of substrate at their surface [45]. Thus, N₂ adsorption/desorption measurements suggests that CM-773 catalyst possesses higher specific surface area and larger pore volumes, which are the advantage for the catalytic oxidation of benzylamine.

To understand the surface morphology of CM-773 and CM-1073 catalysts, FE-SEM studies were performed, and the results are shown in Fig. S2. The FE-SEM images of both catalysts clearly indicate that the samples consist of spherical shaped nanosized particles with some agglomeration of the primary nanoparticles. However, in the case of CM-1073 sample, the size of the particles increases compared to CM-773 due to high temperature treatment. The elemental analysis (EDX) pattern of CM-773 and CM-1073 is shown in C-D parts in Fig. S2, which clearly indicate the presence of Ce, Mn and O as the chemical components in the samples. No trace amount of other impurities could be seen in the detection limit of the EDX which also supports the doping of Mn in the ceria lattice. Further, the EDS mapping of CM-773 and CM-1073 nanostructures is shown in Fig. S3, which unambiguously confirms the uniform distribution of Ce, Mn and O elements on the entire surface of the materials.

Fig. 2 shows TEM images of the CeO₂, CM-773, and CM-1073 samples, respectively. The shape of the CeO₂ particles in pure CeO₂ shows agglomerated quasi-spherical morphology and they are in nonuniform nature. On the contrary, the CeO₂-MnO_x catalysts show homogeneously distributed particles with a mixed morphology of spherical and

hexagonal. The magnified images in the inset in Figs. 2B and C show the nanoparticles with hexagonal structure. It can be seen from Fig. 2A, that the particle sizes of CeO₂ is about ~10-11 nm, which is close to the value obtained from the Scherrer equation. In the case of CM-773 and CM-1073, the TEM images show that the particle size is about ~6-9 and ~15-20 nm, respectively. Further, the size of the nanoparticles in CM-773 and CM-1073 catalysts is fairly evidenced by their histograms of the particle size distribution as calculated from the TEM analysis, which are shown in Fig. S4. It is also obvious that the particle size of the CM-773 catalysts is smaller than that of CeO₂ (~10-11 nm), which may be due to the formation of Ce-O-Mn solid solution. Figs. 2D and E show the HRTEM images of CM-773 and CM-1073 with a continuous lattice, indicating the high crystalline nature of CeO₂ nanostructures. A lattice spacing of ~0.309 nm, which corresponds to the (111) plane of ceria, was measured from the HRTEM images of both samples [46]. Meanwhile, the presence of lattice fringes with a d-spacing of ~0.661 nm, which is related to the (440) plane of Mn₂O₃ nanoparticles clearly visible in the CM-1073, suggesting that the segregation of manganese oxide from solid solution at high thermal treatment [47]. We did not find any separate phase made from MnO_x in CM-773 which is also evident in our XRD analysis.

Raman spectroscopy appears to be a fruitful characterization method for ceria-based materials, since it gives significant information about the crystal defects such as oxygen vacancies. Fig. S5 shows the vis-Raman spectra of the as prepared samples at an excitation wavelength of 632 nm. It can be clearly seen from the figure that the CeO₂ and Mn-doped CeO₂ nanostructures exhibited a high intense band at around ~454-465 cm⁻¹ that corresponds to a triply degenerate Raman-active phonon of the cubic CeO₂ fluorite phase with the space group *Fm3m* [48]. However, the broadened characteristic peak corresponding to CeO₂ with a visible shift (~11 cm⁻¹) to lower wavenumber on the Raman spectrum of CM-773 catalyst, in comparison to that of pure CeO₂, can be readily observed, suggesting the existence of strong interaction between Ce-O and Mn-O [49]. The red-shift for CM-773 is in agreement with the observation of a smaller lattice parameter. Further, the appearance of a peak at about ~646 cm⁻¹ in CM-773 is attributed to the formation of oxygen vacancies due to the contraction of the lattice by the incorporation of Mn ions that favors the oxygen mobility thus improving the redox properties. A similar observation was reported by Barros et al. for the CeO₂-MnO₂ catalyst system [50]. On the other hand, CM-1073 catalyst shows a slight displacement (~5 cm⁻¹) of the band assigned to CeO₂ with a sharpening and an improved symmetry, attributed to the crystal size of the sample increasing at higher calcination temperature. This

phenomenon implied that a specific amount of Ce-Mn-O solid solution actually exists in the CM-1073 catalysts even though the XRD peaks are not observed to shift to higher 2θ values and a small amount of crystalline MnO_x is observed. In addition to the F_{2g} band, the CM-1073 sample exhibited three bands at ~ 312 , 369 and 655.4 cm^{-1} , indicating the presence of Mn_2O_3 and Mn_3O_4 phases and it is also evident by XRD analysis (shown in Fig. 1) [51]. Interestingly, no MnO_x peaks were noticed in the CM-773 sample, confirming the formation of solid solution, and corroborating the XRD results very well.

To understand the effects of Mn ion doping in ceria on the surface chemical states and identify the chemical status of the metal ions in the samples, XPS measurements were carried out. The results of typical samples are shown in Fig. 3. The fitted XPS spectra of O 1s are shown in Fig. 3A. The three resolved XPS peaks, which are based on the binding energy from lowest to highest, are ascribed to the crystal lattice oxygen (O^{2-} , denoted as O_a), surface adsorbed oxygen (O_2^- , O_2^{2-} , O^- , denoted as O_b) and chemisorbed water and/or carbonates (denoted as O_c), respectively [52]. As shown in Table S2, the surface adsorbed oxygen contents ($\text{O}_b/\text{O}_{\text{total}}$) of CeO_2 , CM-773, and CM-1073 are 30.27, 36.11, and 33.67%, respectively. This result clearly shows that CM-773 has much higher adsorbed oxygen content than CeO_2 and CM-1073. CM-1073 just has higher adsorbed oxygen content than CeO_2 . It has been generally accepted that the surface adsorbed oxygen was more reactive than the lattice oxygen in the oxidation reactions due to its higher mobility [53]. This meant that the CM-773 catalyst might show better activity for the benzylamine oxidation than the CeO_2 catalyst. Additionally, compared with the undoped sample, the O 1s core level BE values of the CM-773 are shifted to a lower energy region. This is assigned to the fact that the Mn^{x+} ions are incorporated into the ceria crystal structure and there are strong interactions between the MnO_x ions and ceria.

Fig. 3B shows the XPS spectra of Ce 3d for CeO_2 -containing samples. The Ce 3d region is composed of 5 spin-orbit doublets and these are commonly denoted by u and v, which represent the $3d_{3/2}$ and $3d_{5/2}$ states, respectively, in the range 880–920 eV. The photoelectron peaks were analyzed by Gaussian peak fitting. Ten peaks corresponding to the pairs of spin-orbit doublets can be identified in the Ce $3d_{3/2}$ and $3d_{5/2}$ spectra, which is in good agreement with other research [54]. Specifically, v_o , v' , u_o and u' belong to Ce^{3+} species, whereas v , v'' , v''' , u , u'' and u''' belong to Ce^{4+} species. As can be seen, the chemical valence of cerium on the surface of our samples was a mixed valence state, and was mainly Ce^{4+} as well as small fraction of Ce^{3+} . The relative amount of surface Ce^{3+} could be determined by

$\text{Ce}^{3+}/(\text{Ce}^{3+}+\text{Ce}^{4+})$, where $\text{Ce}^{3+} = (v_o+v'+u_o+u')$ and $\text{Ce}^{4+} = (v+v''+v''' +u+u''+u''')$ and the results are shown in Table S2 [55]. The comparatively higher amount of Ce^{3+} present in CM-773 nanoparticles (Table S2) can be attributed to the introduction of Mn that resulted in immense conversion of Ce^{4+} to Ce^{3+} on the catalyst surface compared to that on CeO_2 and CM-1073. As a result of high-valent Ce^{3+} ion, oxygen vacancies are created which accumulates a large number of adsorbed oxygen on the surface [56]. This observation is in good accordance with the Raman and O 1s results and demonstrates that the surface adsorbed oxygen species have a close relation with Ce^{3+} species concentration. Interestingly, the Ce 3d peaks of CM-773 are slightly shifted to lower binding energy side in comparison to other samples. This is probably due to the change in the chemical environment of Ce-O atoms which caused a change in the coordination number and hence in the binding energies.

The Mn 2p XPS spectra of MnO_x and Mn-doped ceria samples calcined at 773 and 1073 K temperatures are shown in Fig. 3C. Mn 2p spectrum is characterized by the doublet of two spin-orbit components, namely, Mn 2p_{3/2} and Mn 2p_{1/2}. The binding energies of Mn 2p_{3/2} and Mn 2p_{1/2} were ~641.6 and ~653.3 eV, respectively [57]. On the basis of the binding energies of the Mn 2p main lines, as shown in figure, it is difficult to determine the oxidation states of Mn cations because similar values can be obtained for most of the Mn oxides (e.g. MnO, Mn_2O_3 , and MnO_2). Hence, the Mn 2p_{3/2} peak is fitted with a Shirley background and Gaussian-Lorentz model functions, and three peaks at 641.5, 642.6 and 644.3 eV can be obtained, based on standard binding energies and previous literature [58, 59]. The observed binding energies suggest the co-existence of Mn^{2+} , Mn^{3+} and Mn^{4+} ions on the surface of samples. The concentration of $\text{Mn}^{4+}/\text{Mn}_{\text{total}}$ in MnO_x , CM-773, and CM-1073 are shown in Table S2. It can be clearly seen from the Table S2 that the nanostructured CM-773 exhibits higher valent Mn species on its surface than CM-1073, which allows it to be much superior catalytic system for benzylamine reaction. From the above, although the same chemical component in the two ceria-manganese samples, the different calcination temperatures result in the diverse oxidation state for the surface Mn species, particular with Mn^{4+} . Further, the main peak of the Mn 2p_{3/2} state becomes broader and shifts to higher binding energy with increasing calcination temperature, which may be attributed to the weaker interaction between ceria and manganese oxides.

One of the other major factors having a noticeable effect on the catalytic performance of a metal oxide catalyst is its redox property. Hence, the H_2 -TPR analysis was conducted on the as-prepared samples to reveal their redox properties and the comparative profiles of all the

samples are illustrated in Fig. 4. It can be seen that the reduction of CeO_2 occurs in two consecutive steps at ~ 765 and 1065 K, which are due to the reduction of the surface active oxygen, and the second peak corresponding to the reduction of bulk oxygen, respectively [60]. The profile of pure MnO_x shows a peak centered at ~ 603 K, which can be assigned to the reduction of MnO_2 to Mn_3O_4 , whereas the peak at ~ 747 K is attributed to the transformation of Mn_3O_4 to MnO [61]. When ceria is doped with manganese, the TPR profiles of the mixed oxides showed three reduction peaks; the first peak (α) around $512\text{--}520$ K was related to the MnO_2 to Mn_3O_4 on the surface; the second peak (β) around $603\text{--}654$ K was assigned to the overlapping of the surface reduction of Ce^{4+} and the reduction of Mn_3O_4 to MnO ; and the last peak (γ) at $1048\text{--}1055$ was associated with the reduction of bulk ceria [62]. When comparing with the individual oxides, the mutual promotion effect could improve the reducibility of both CeO_2 and MnO_x by shifting reduction peaks toward lower temperatures, in particular with surface reduction (β). This region of the profile is of particular interest for low temperature catalytic oxidation reactions. The order of surface reduction temperature is as follows: $\text{CM-773} < \text{CM-1073} < \text{CeO}_2$. The decreased reduction temperature in CM-773 attributed to the synergistic effect between the manganese and cerium oxides through the formation of a Ce-O-Mn solid solution with maximum -Ce-O-Mn- bonds, which can create oxygen defects and structural distortion [63]. Therefore, a higher concentration of these surface defects can be expected for CM-773. This is in good agreement with the results of the Raman and XPS analyses. It can be clearly seen that the shift of bulk reduction peak in both CM-773 and CM-1073 samples is not pronounced which probably indicates that Mn cations are mainly localized at the surface layers. However, compared with pure ceria and CM-1073, the CM-773 shows this peak at lower temperature. On the other hand, the CM-1073 sample shows an extra peak with low intensity (δ) at ~ 589 K and this peak may be related to Mn_2O_3 phase, which is consistent with the XRD, Raman and HRTEM results. Furthermore, it is evident that with an increase in calcination temperature, the reduction curves shift gradually towards higher temperature which indicated that the oxidation ability of the catalysts was decreased. The segregation of dopant cations of the surface and domain boundaries of ceria is a well-known phenomenon at higher calcination temperature; thereby interaction of Ce-Mn in the bulk is less thus making it hard to reduce Ce^{4+} to Ce^{3+} . The difference in the low temperature reducible properties on the two $\text{CeO}_2\text{-MnO}_x$ catalysts might lead to the distinction of their catalytic performances.

The identification and characterization of the acidic properties on the surface of metal oxides is of significant fundamental interest in oxidation reactions. Temperature programmed desorption is one of the most widely used and flexible techniques for characterizing these properties on oxide surfaces, where NH_3 was used as the probe molecule. Fig. S6 shows the NH_3 -TPD curves of CM-773 and CM-1073 samples. As shown in Fig. S6, the shapes of the NH_3 -TPD patterns of the both samples were similar with small differences and three desorption peaks were observed between ~ 350 - 950 K due to the variability of adsorbed NH_3 species with different thermal stabilities. Two broad peaks spanned in the temperature range of ~ 375 - 535 and ~ 550 - 740 K were observed and these peaks could be assigned to successive desorption of NH_3 by weak and medium strength acidic sites, respectively. There is one strong and broad peak at around ~ 835 K, which corresponds to strong acidic sites [64]. A closer look at the figure revealed that as the calcination temperature increases, the intensity of the NH_3 desorption peaks decreases and shifted to higher temperature which indicates that the surface acidic sites on the CM-1073 mixed oxide became weaker. Thus, we can conclude that there are high amounts and uniform acidic centers on the CM-773 mixed oxide, which are believed to be significantly beneficial to benzylamine oxidation reaction.

3.2 Catalytic activity studies

In order to determine the catalytic oxidation properties of synthesized catalysts, oxidation of benzylamine was used as a model reaction and the reaction was carried out in the presence of as prepared catalysts without solvent for 2 h at 393 K and atmospheric pressure. A graphical illustration of the results obtained is given in Fig. 5. It can be clearly seen from the Fig. 5A that approximately 8, 14, 54, and 71% of benzylamine conversions were obtained over the CeO_2 , MnO_x , CM-1073 and CM-773 catalysts, respectively. On the other hand, very low benzylamine conversion ($\sim 3\%$) was noticed in the absence of catalyst under similar conditions. This observation plainly indicates the importance of a catalyst for the oxidation of benzylamine. Remarkably, a high selectivity of dibenzylimine (~ 99.7 – 99.8%) was found, along with insignificant amounts of benzonitrile (~ 0.2 – 0.3%) for all the catalysts. The CeO_2 - MnO_x mixed oxides calcined at 773 and 1073 K showed an enhanced catalytic activity in the reaction, compared to the pure CeO_2 and MnO_x oxides, which is ascribed to the formation of a Ce-O-Mn solid solution with enhanced catalytic properties. Amongst the CeO_2 - MnO_x composite oxides, the CM-773 gave the best performance considering the conversion of benzylamine. The better catalytic activity of CM-773 could be ascribed to the following reasons; The XRD result indicated that Mn-doping significantly altered the lattice parameter

of the fluorite structure of CeO_2 through the formation of pure Ce-O-Mn solid solution, and formation of higher quantity of oxygen vacancies was observed from Raman study. The BET results indicated that the reactants and products easily diffuse from the catalyst surface due to the higher surface area of mesostructured CM-773. The incorporation of Mn^{x+} in the ceria lattice increased the concentration of Ce^{3+} species. These Ce^{3+} species are paramagnetic in nature which can interact with the molecular oxygen and further activate it for the oxidation reaction. Hence, the increase in Ce^{3+} content and the presence of Mn^{x+} in the ceria lattice, as evidenced from XPS results may further increase the lattice oxygen mobility and oxygen chemisorption at the catalyst surface. TPR results show that Mn-doping lower the reduction temperature due to the synergistic effect between Ce and Mn, whereas NH_3 -TPD results also revealed that surface acidity of CeO_2 increased with Mn doping. So, the current catalytic performance tests suggested that the insertion of Mn into ceria could remarkably improve the benzylamine oxidation.

Since the CM-773 catalyst showed a better performance, it was used for further investigation of the effect of reaction conditions on performance. In order to recognize the effect of temperature on the aerobic oxidation of benzylamine, we have performed the reaction with different reaction temperatures from 313 to 393 K over the CM-773 using O_2 under solvent-free conditions. The achieved results are shown in Fig. 5B. Obviously, the reaction temperature exhibited a significant impact on the reaction. It can be clearly seen that the conversion of benzylamine consistently increases from ~5, 12, 23, 55, and 71% with the increase of reaction temperature from 313, 333, 353, 373, and 393 K, respectively. Notably there was no significant variation in the dibenzylimine selectivity (99.7-99.8%) with the reaction temperature. Further increasing the temperature from 393 to 403 K, we did not observe significant variation in the conversion of benzylamine (75%) and dibenzylimine selectivity (~99.5%). These interesting observations suggest that the temperature 393 K is the optimum temperature and hence it was selected for further studies. The effect of reaction time on the oxidation of benzylamine is demonstrated in Fig. 6A. Clearly, as the reaction proceeded, the benzylamine conversion was increased. The achieved benzylamine conversions are ~ 30, 71, and 96% for 1, 2, and 3 h of reaction times, respectively. On the other hand, no considerable variation in the dibenzylimine selectivity (~99.7-99.8%) was noted with the reaction time. Thus, the suitable reaction time was chosen as 2 h in this investigation.

The effect of catalyst amount towards oxidation of benzylamine was studied by using CM-773 from 20 to 100 mg and the obtained results are shown in Fig. S7. It can be clearly notified that the conversion of benzylamine was gradually increased with respect to the amount of catalyst and the high conversion of benzylamine was achieved at 100 mg of catalyst but, no appreciable change in the dibenzylimine selectivity (~99.6-99.8%) was observed. The enhancement in the conversion of benzylamine with the weight of catalyst could be endorsed to availability of more number of active sites for contributing in the reaction and enhancing conversion of benzylamine. Hence, the amount of catalyst showed noteworthy effect in the benzylamine oxidation and the suitable catalyst amount was chosen as 100 mg in the present case.

We also examined the scope of the CM-773 catalyst for the oxidative coupling of various substituted benzylamines using molecular O₂ under solvent-free conditions. The achieved results are summarized in Table 2. In general, a variety of substituted benzylamines with either electron-withdrawing or -donating groups can be selectively converted into the respective imines using the CM-773. As expected, the CM-773 shows an outstanding efficiency in converting the substituted benzylamines into the corresponding dibenzylamines. This observation suggests that the electronic properties of the substituents show a diminutive effect on the efficiency of the CM-773 in the benzylamine oxidation. In contrast, low amine conversion was found for the *o*-chloro substituted benzylamine (69%) compared with the *p*-chloro substituted benzylamine (76%, Table 2, entries 11-12). These results indicate that the reaction is sensitive to the steric hindrance of the substituents. Despite the nature of the substituent and its position on the benzylamine, almost 99.5-99.8% selectivity of the imine product was achieved with the CM-773 catalyst. To our delight, we found the general applicability of this conversion for secondary amine and cyclic secondary amines (Table 3, entries 1-3).

Finally, the efficiency of CM-773 catalyst was studied up to 6 cycles to evaluate its reusability and stability for the oxidation of benzylamine. The obtained results are presented in Fig. 6B. The reaction conditions employed include benzylamine (0.2 mmol), catalyst amount (100 mg), O₂ pressure 1 atm, reaction time (3 h), and temperature 393 K. After completion of each cycle, the catalyst was filter out from the reaction mixture by simple centrifugation. The solid catalyst was washed several times with methanol to remove impurities and dried at 393 K for 3 h. It can be concluded from the figure that there was no significant decrease in the conversion and selectivity up to 5 cycles. Afterwards, a slight

variation in the catalytic activity was found which might be attributed to change in the structural properties of the catalyst, which are responsible for exposing the less active sites on the surface. Overall, the investigated catalyst has good stability during catalytic activity.

A possible mechanism was proposed for the aerobic oxidation of benzylamine to dibenzylimine over the CM-773 (Scheme 1) [16, 65-66]. As shown in Scheme 1, an imine intermediate can be formed from the oxidative dehydrogenation of benzylamine. This unstable imine intermediate reacts with another benzylamine to form an aminal product, which subsequently release NH_3 molecule to give the dibenzylimine product. As shown in Scheme 1, small amount of benzonitrile (0.1–0.5 %) was found in this study, which is due to the consecutive oxidative dehydrogenation of the imine intermediate.

Conclusions

In summary, nanosized Mn-doped solid solution catalysts were successfully synthesized via an easily performable coprecipitation method and evaluated their activity for the oxidation of benzylamine using O_2 as a green oxidant under solvent-free conditions. The doping of Mn finely tunes the structural, textural and chemical properties of the pure cerium oxide. Among all the catalysts, the CM-773 catalyst displays a remarkable improvement in terms of the activity and stability compared to pure CeO_2 and MnO_x . Based on our characterization results, it is believed that the enhanced benzylamine oxidation activity of CM-773 is attributable to the presence of a large amount of oxygen vacancy defects, perhaps as a consequence of the formation of Ce-O-Mn solid solution through the synergetic interaction between ceria and MnO_x in this catalyst. This conclusion is further supported by its superior BET surface area, higher amount of surface adsorbed oxygen, low temperature reducibility and high concentration of strong acidic sites. Various reaction parameters, such as reaction time, temperature, catalyst amount and reusability were studied for oxidation of benzylamine to optimize the reaction conditions. A remarkable observation noticed in this study is that the CM-773 catalyst shows an outstanding performance in terms of benzylamine conversion (~71%) and selectivity of dibenzylimine product (~99.8%) for 2 h at 393 K.

Supporting Information Available

Detailed information about the chemical compositions, the surface atomic concentrations, N_2 adsorption–desorption isotherms, FESEM-EDX, EDX elemental mapping analysis, histogram of the particle size distributions, Raman spectra, NH_3 -TPD profiles and the effect of CM-773 catalyst amount on the oxidation of benzylamine results of the investigated catalysts are

summarized in Table S1, Table S2, Figure S1, Figure S2, Figure S3, Figure S4, Figure S5 and Figure S6, Figure S7, respectively.

Acknowledgements

A.R and P.V gratefully acknowledge the University Grants Commission (UGC), New Delhi for financial assistance under UGC-SRF and DSKPDF schemes, respectively.

References

- [1] S. Ahmad, K. Gopalaiah, S.N. Chandrudu, R. Nagarajan, Anion (fluoride)-doped ceria nanocrystals: synthesis, characterization, and its catalytic application to oxidative coupling of benzylamines, *Inorg. Chem.* 53 (2014) 2030–2039.
- [2] D. Ge, G. Qu, X. Li, K. Geng, X. Cao, H. Gu, Novel transition bimetal-organic frameworks: recyclable catalyst for the oxidative coupling of primary amines to imines at mild conditions, *New J. Chem.* 40 (2016) 5531–5536.
- [3] B. Chen, J. Li, W. Dai, L. Wang, S. Gao, Direct imine formation by oxidative coupling of alcohols and amines using supported manganese oxides under an air atmosphere, *Green Chem.* 16 (2014) 3328–3334.
- [4] C. Su, R. Tandiana, J. Balapanuru, W. Tang, K. Pareek, C.T. Nai, T. Hayashi, K.P. Loh, Tandem catalysis of amines using porous graphene oxide, *J. Am. Chem. Soc.* 137 (2015) 685–690.
- [5] L. Tang, H. Sun, Y. Li, Z. Zha, Z. Wang, Highly active and selective synthesis of imines from alcohols and amines or nitroarenes catalyzed by Pd/DNA in water with dehydrogenation, *Green Chem.* 14 (2012) 3423–3428.
- [6] C.M. Opris, O.D. Pavel, A. Moragues, J. El Haskourib, D. Beltran, P. Amoros, M.D. Marcos, L.E. Stoflea, V.I. Parvulescu, New multicomponent catalysts for the selective aerobic oxidative condensation of benzylamine to N-benzylidenebenzylamine, *Catal. Sci. Technol.* 4 (2014) 4340–4355.
- [7] S. Furukawa, A. Suga, T. Komatsu, Highly efficient aerobic oxidation of various amines using Pd₃Pb intermetallic compounds as catalysts, *Chem. Commun.* 50 (2014) 3277–3280.

- [8] S. Kobayashi, Y. Mori, J.S. Fossey, M.M. Salter, Catalytic enantio selective formation of C-C bonds by addition to imines and hydrazones: A ten-year update, *Chem. Rev.* 111 (2011) 2626–2704.
- [9] K.C. Nicolaou, C.J.N. Mathison, T. Montagnon, o-Iodoxybenzoic acid (IBX) as a viable reagent in the manipulation of nitrogen- and sulfur-containing substrates: scope, generality, and mechanism of IBX-mediated amine oxidations and dithiane deprotections, *J. Am. Chem. Soc.* 126 (2004) 5192–5201.
- [10] K.C. Nicolaou, C.J.N. Mathison, T. Montagnon, New reactions of IBX: oxidation of nitrogen- and sulfur-containing substrates to afford useful synthetic intermediates, *Angew. Chem. Int. Ed.* 42 (2003) 4077–4082.
- [11] S. Furukawa, Y. Ohno, T. Shishido, K. Teramura, T. Tanaka, Selective amine oxidation using Nb₂O₅ Photocatalyst and O₂, *ACS Catal.* 1 (2011) 1150–1153.
- [12] C. Hammond, M.T. Schimperli, I. Hermans, Insights into the oxidative dehydrogenation of amines with nanoparticulate iridium oxide, *Chem. Eur. J.* 19 (2013) 13193–13198.
- [13] P. Sudarsanam, B. Hillary, M.H. Amin, S.B.A. Hamid, S.K. Bhargava, Structure-activity relationships of nanoscale MnO_x/CeO₂ hetero structured catalysts for selective oxidation of amines under eco-friendly conditions, *Appl. Catal. B* 185 (2016) 213–224.
- [14] F. Li, J. Chen, Q. Zang, Y. Wang, Hydrous ruthenium oxide supported on Co₃O₄ as efficient catalyst for aerobic oxidation of amines, *Green Chem.* 10 (2008) 553–562.
- [15] S. Zhao, C. Liu, Y. Guo, J.C. Xiao, Q.Y. Chen, Oxidative coupling of benzylamines to imines by molecular oxygen catalyzed by Cobalt(II) β -tetrakis (trifluoromethyl)-mesotetraphenylporphyrin, *J. Org. Chem.* 79 (2014) 8926–8931.
- [16] P. Sudarsanam, P.R. Selvakannan, S.K. Soni, S.K. Bhargava, B.M. Reddy, Structural evaluation and catalytic performance of nano-Au supported on nanocrystalline Ce_{0.9}Fe_{0.1}O_{2- δ} solid solution for oxidation of carbon monoxide and benzylamine, *RSC Adv.* 4 (2014) 43460–43469.
- [17] S.K. Klitgaard, K. Egeblad, U.V. Mentzel, A.G. Popov, T. Jensen, E. Taarning, I.S. Nielsen, C.H. Christensen, Oxidations of amines with molecular oxygen using bifunctional gold–titania catalysts, *Green Chem.* 10 (2008) 419–423.
- [18] R.D. Patil, S. Adimurthy, Copper(0)-catalyzed aerobic oxidative synthesis of imines from amines under solvent-free conditions, *RSC Adv.* 2 (2012) 5119–5122.
- [19] C. Sun, D. Xue, Size-dependent oxygen storage ability of nano-sized ceria, *Phys. Chem. Chem. Phys.* 15(2013) 14414–14419.

- [20] P. Sudarsanam, B. Mallesham, A. Rangaswamy, B.G. Rao, S.K. Bhargava, B.M. Reddy, Promising nanostructured gold/metal oxide catalysts for oxidative coupling of benzylamines under eco-friendly conditions, *J. Mol. Catal. A: Chem.* 412 (2016) 47–55.
- [21] C. Sun, X. Li, H. Wang, D. Xue, Crystallization-Dependent Luminescence Properties of Ce:LuPO₄, *Inorg. Chem.* 55 (2016) 2969–2976.
- [22] X. Wang, D. Liu, J. Li, J. Zhen, H. Zhang, Clean synthesis of Cu₂O@CeO₂ core@shell nanocubes with highly active interface, *NPG Asia Mater.* 7 (2015) e158.
- [23] P. Sudarsanam, A. Rangaswamy, B.M. Reddy, An efficient noble metal-free Ce–Sm/SiO₂ nano-oxide catalyst for oxidation of benzylamines under ecofriendly conditions, *RSC Adv.* 4 (2014) 46378–46382.
- [24] S. Mallick, S. Rana, K. Parida, Facile Method for the Synthesis of Phosphomolybdic Acid Supported on Zirconia–Ceria Mixed Oxide and Its Catalytic Evaluation in the Solvent-Free Oxidation of Benzyl Alcohol, *Ind. Eng. Chem. Res.* 51 (2012) 7859–7866.
- [25] L. Ilieva, G. Pantaleo, I. Ivanov, R. Zanella, A.M. Venezia, D. Andreeva, A comparative study of differently prepared rare earths-modified ceria-supported gold catalysts for preferential oxidation of CO, *Int. J. Hydrogen Energy* 34 (2009) 6505–6515.
- [26] A. Longo, L.F. Liotta, G. Pantaleo, F. Giannici, A.M. Venezia, A. Martorana, Structure of the Metal-Support Interface and Oxidation State of Gold Nanoparticles Supported on Ceria, *J. Phys. Chem. C* 116 (2012) 2960–2966.
- [27] K. Chen, D. Xue, In-situ electrochemical route to aerogel electrode materials of graphene and hexagonal CeO₂, *J. Colloid Interface Sci.* 446 (2015) 77–83.
- [28] K. Chen, D. Xue, Water-soluble inorganic salt with ultrahigh specific capacitance: Ce(NO₃)₃ can be designed as excellent pseudo capacitor electrode, *J. Colloid Interface Sci.* 416 (2014) 172–176.
- [29] C. Kun Feng, X. Dong Feng, Rare earth and transitional metal colloidal supercapacitors, *Science China Technol. Sci.* 58 (2015) 1768–1778.
- [30] X. Wang, Y. Zhang, S. Song, X. Yang, Z. Wang, R. Jin, H. Zhang, L-Arginine-Triggered self-Assembly of CeO₂ Nanosheaths on Palladium Nanoparticles in Water, *Angew. Chem. Int. Ed.* 55 (2016) 4542–4546.
- [31] P. Venkataswamy, K.N. Rao, D. Jampaiah, B.M. Reddy, Nanostructured manganese doped ceria solid solutions for CO oxidation at lower temperatures, *Appl. Catal. B* 162 (2015) 122–132.

- [32] X. Wang, D. Liu, J. Li, J. Zhen, F. Wang, H. Zhang, γ - Al_2O_3 supported Pd@ CeO_2 core@shell nanospheres: salting-out assisted growth and self assembly, and their catalytic performance in CO oxidation, *Chem. Sci.*, 6 (2015) 2877–2884.
- [33] P. Venkataswamy, D. Jampaiah, K.N. Rao, B.M. Reddy, Nanostructured $\text{Ce}_{0.7}\text{Mn}_{0.3}\text{O}_{2-\delta}$ and $\text{Ce}_{0.7}\text{Fe}_{0.3}\text{O}_{2-\delta}$ solid solutions for diesel soot oxidation, *Appl. Catal. A: Gen.*, 488 (2014) 1–10.
- [34] K. Chen, W. Pan, D. Xue, Phase Transformation of Ce^{3+} Doped MnO_2 for Pseudocapacitive Electrode Materials, *J. Phys. Chem. C* 120 (2016) 20077–20081.
- [35] D. Jampaiah, S.J. Ippolito, Y.M. Sabri, B.M. Reddy, S.K. Bhargava, Highly efficient nanosized Mn and Fe codoped ceria-based solid solutions for elemental mercury removal at low flue gas temperatures, *Catal. Sci. Technol.* 5 (2015) 2913–2924.
- [36] X. Wang, D. Liu, S. Song, H. Zhang, Pt@ CeO_2 Multicore@Shell Self-Assembled Nanospheres: Clean Synthesis, Structure Optimization, and Catalytic Applications, *J. Am. Chem. Soc.* 135 (2013) 15864–15872.
- [37] X. Yu, J. Li, Y. Wei, Z. Zhao, J. Liu, B. Jin, A. Duan, G. Jiang, Three-dimensionally ordered macroporous $\text{Mn}_x\text{Ce}_{1-x}\text{O}_\delta$ and Pt/ $\text{Mn}_{0.5}\text{Ce}_{0.5}\text{O}_\delta$ catalysts: synthesis and catalytic performance for soot oxidation, *Ind. Eng. Chem. Res.* 53 (2014) 9653–9664.
- [38] Y. Tang, H. Qiao, H. Wang, P. Tao, Nanoparticulate $\text{Mn}_{0.3}\text{Ce}_{0.7}\text{O}_2$: a novel electrocatalyst with improved power performance for metal/air batteries, *J. Mater. Chem. A* 1 (2013) 12512–12518.
- [39] X. Tang, Y. Li, X. Huang, Y. Xu, H. Zhu, J. Wang, W. Shen, MnO_x - CeO_2 mixed oxide catalysts for complete oxidation of formaldehyde: Effect of preparation method and calcination temperature, *Appl. Catal. B* 62 (2006) 265–273.
- [40] C. Xia, C. Hu, P. Chen, B. Wan, X. He, Y. Tian, Magnetic properties and photoabsorption of the Mn-doped CeO_2 nanorods, *Mater. Res. Bull.* 45 (2010) 794–798.
- [41] S. Deng, H. Liu, W. Zhou, J. Huang, G. Yu, Mn-Ce oxide as a high-capacity adsorbent for fluoride removal from water, *J. Hazard. Mater.* 186 (2011) 1360–1366.
- [42] Z.Q. Zou, M. Meng, Y.Q. Zha, Surfactant-assisted synthesis, characterizations, and catalytic oxidation mechanisms of the mesoporous MnO_x - CeO_2 and Pd/ MnO_x - CeO_2 catalysts used for CO and C_3H_8 oxidation, *J. Phys. Chem. C* 114 (2010) 468–477.
- [43] K.S.W. Sing, D.H. Everett, R.A.W. Haul, Reporting physisorption data for gas/solid systems with special reference to the determination of surface area and porosity, *Pure Appl. Chem.* 57 (1985) 603–619.

- [44] S.K. Meher, G.R. Rao, Tuning, via counter anions, the morphology and catalytic activity of CeO₂ prepared under mild conditions, *J. Colloid Interface Sci.* 373 (2012) 46–56.
- [45] J.H. Pan, H. Dou, Z. Xiong, C. Xu, J. Ma, X.S. Zhao, Porous photocatalysts for advanced water purifications, *J. Mater. Chem.* 20 (2010) 4512–4528.
- [46] J. Zhang, Y. Cao, C.A. Wang, R. Ran, Design and preparation of MnO₂/CeO₂-MnO₂ Double-shelled binary oxide hollow spheres and their application in CO oxidation *ACS Appl. Mater. Interfaces.* 8 (2016) 8670–8677.
- [47] S. Cao, N. Han, J. Han, Y. Hu, L. Fan, C. Zhou, R. Guo, Mesoporous Hybrid Shells of Carbonized Polyaniline/Mn₂O₃ as Non-Precious Efficient Oxygen Reduction Reaction Catalyst *ACS Appl. Mater. Interfaces.* 8 (2016) 6040–6050.
- [48] M. Zhang, D. Jiang, H. Jiang, Enhanced oxygen storage capacity of Ce_{0.88}Mn_{0.12}O_y compared to CeO₂: An experimental and theoretical investigation, *Mater. Res. Bull.* 47 (2012) 4006–4012.
- [49] L. Liu, J. Shi, X. Zhang, J. Liu, Flower-like Mn-doped CeO₂ microstructures: synthesis, characterizations and catalytic properties, *J. Chem.* 2015 (2015) 254750–254760.
- [50] F.A.A. Barros, H.S.A. de Sousa, A.C. Oliveira, M.C. Junior, J.M. Filho, B.C. Viana, A.C. Oliveira, Characterisation of high surface area nanocomposites for glycerol transformation: Effect of the presence of silica on the structure and catalytic activity, *Catal. Today* 212 (2013) 127–136.
- [51] B. Guan, H. Lin, L. Zhu, Z. Huang, Selective catalytic reduction of NO_x with NH₃ over Mn, Ce Substitution Ti_{0.9}V_{0.1}O_{2-δ} nanocomposites catalysts prepared by self-propagating high-temperature synthesis method, *J. Phys. Chem. C* 115 (2011) 12850–12863.
- [52] X. Xing, Y. Cai, N. Chen, Y. Li, D. Deng, Y. Wang, Synthesis of mixed Mn-Ce-O_x one dimensional nanostructures and their catalytic activity for CO oxidation, *Ceram. Int.* 41 (2015) 4675–4682.
- [53] J. Fang, X. Bi, D. Si, Z. Jiang, W. Huang, Spectroscopic studies of interfacial structures of CeO₂-TiO₂ mixed oxides. *Appl. Surf. Sci.* 253 (2007) 8952–8961.
- [54] B.C. Mohanty, J.W. Lee, D.-H. Yeon, Y.-H. Jo, J.H. Kim, Y.S. Cho, Dopant induced variations in microstructure and optical properties of CeO₂ nanoparticles, *Mater. Res. Bull.* 46 (2011) 875–883.
- [55] Z. Wangcheng, Z. Xinye, G. Yanglong, W. Li, G. Yun, L. Guanzhong, Synthesis of mesoporous CeO₂-MnO_x binary oxides and their catalytic performances for CO oxidation, *J. Rare Earths* 32 (2014) 146–152.

- [56] J. He, G.K. Reddy, S.W. Thiel, P.G. Smirniotis, N.G. Pinto, Ceria-modified manganese oxide/titania materials for removal of elemental and oxidized mercury from flue gas, *J. Phys. Chem. C* 115 (2011) 24300–24309.
- [57] Y.F. Han, F. Chen, Z. Zhong, K. Ramesh, L. Chen, E. Widjaja, Controlled synthesis, characterization, and catalytic properties of Mn_2O_3 and Mn_3O_4 nanoparticles supported on mesoporous silica SBA-15, *J. Phys. Chem. B* 110 (2006) 24450–24456.
- [58] G. Qi, R.T. Yang, Characterization and FT-IR Studies of $\text{MnO}_x\text{-CeO}_2$ catalyst for low-temperature selective catalytic reduction of NO with NH_3 , *J. Phys. Chem. B* 108 (2004) 15738–15747.
- [59] Z. Chen, Q. Yang, H. Li, X. Li, L. Wang, S.C. Tsang, Cr– MnO_x mixed-oxide catalysts for selective catalytic reduction of NO_x with NH_3 at low temperature, *J. Catal.* 276 (2010) 56–65.
- [60] G. Picasso, R. Cruz, M.R.S. Kou, Preparation by co-precipitation of Ce–Mn based catalysts for combustion of n-hexane, *Mater. Res. Bull.* 70 (2015) 621–632.
- [61] X. Xiao, Z. Sheng, L. Yang, F. Dong, Low-temperature selective catalytic reduction of NO_x with NH_3 over a manganese and cerium oxide/graphene composite prepared by a hydrothermal method, *Catal. Sci. Technol.* 6 (2016) 1507–1514.
- [62] F. Lin, Y. He, Z. Wang, Q. Ma, R. Whiddon, Y. Zhu, J. Liu, Catalytic oxidation of NO by O_2 over $\text{CeO}_2\text{-MnO}_x$: SO_2 poisoning mechanism, *RSC Adv.* 6 (2016) 31422–31430.
- [63] P. Zhang, H. Lu, Y. Zhou, Z. Li, Z. Wu, S. Yang, H. Shi, Q. Zhu, Y. Chen, S. Dai, *Nat. Comm.* 2015, DOI: 10.1038/ncomms9446.
- [64] Y. Xiong, C. Tang, X. Yao, L. Zhang, L. Li, X. Wang, Y. Deng, F. Gao, L. Dong, Effect of metal ions doping ($\text{M} = \text{Ti}^{4+}$, Sn^{4+}) on the catalytic performance of $\text{MnO}_x/\text{CeO}_2$ catalyst for low temperature selective catalytic reduction of NO with NH_3 , *Appl. Catal. A* 495 (2015) 206–216.
- [65] B. Chen, L. Wang, W. Dai, S. Shang, Y. Lv, S. Gao, Metal-free and solvent-free oxidative coupling of amines to imines with mesoporous carbon from macrocyclic compounds, *ACS Catal.* 5 (2015) 2788–2794.
- [66] X.J. Yang, B. Chen, X.B. Li, L.-Q. Zheng, L.Z. Wu, C.H. Tung, Photocatalytic organic transformation by layered double hydroxides: highly efficient and selective oxidation of primary aromatic amines to their imines under ambient aerobic conditions, *Chem. Commun.* 50 (2014) 6664–6667.

Captions for figures

Fig. 1. Powder XRD patterns of pure CeO_2 and MnO_x calcined at 773 K and $\text{Ce}_{0.7}\text{Mn}_{0.3}\text{O}_{2-\delta}$ (CM) samples calcined at 773 and 1073 K.

Fig. 2. TEM images pure CeO_2 calcined at 773 K and $\text{Ce}_{0.7}\text{Mn}_{0.3}\text{O}_{2-\delta}$ (CM) samples calcined at 773 and 1073 K (A, B, C), and HRTEM images of $\text{Ce}_{0.7}\text{Mn}_{0.3}\text{O}_{2-\delta}$ (CM) samples calcined at 773 and 1073 K (D, E) (inset: enlarged views of selected areas).

Fig. 3. (A) O 1s core level XPS spectra of pure CeO_2 calcined at 773 K and $\text{Ce}_{0.7}\text{Mn}_{0.3}\text{O}_{2-\delta}$ (CM) samples calcined at 773 and 1073 K. (B) Ce 3d XP spectra of pure CeO_2 calcined at 773 K and $\text{Ce}_{0.7}\text{Mn}_{0.3}\text{O}_{2-\delta}$ (CM) samples calcined at 773 and 1073 K. (C) Mn 2p XP spectra of pure MnO_x calcined at 773 K and $\text{Ce}_{0.7}\text{Mn}_{0.3}\text{O}_{2-\delta}$ (CM) samples calcined at 773 and 1073 K.

Fig. 4. H_2 -TPR profiles pure CeO_2 and MnO_x calcined at 773 K and $\text{Ce}_{0.7}\text{Mn}_{0.3}\text{O}_{2-\delta}$ (CM) samples calcined at 773 and 1073 K.

Fig. 5. (A) Selective oxidation of benzylamine over pure CeO_2 and MnO_x calcined at 773 K, and $\text{Ce}_{0.7}\text{Mn}_{0.3}\text{O}_{2-\delta}$ (CM) samples calcined at 773 and 1073 K. Reaction conditions: benzylamine (0.2 mmol), time (2 h), temperature (393 K), catalyst amount (100 mg), and O_2 balloon. (B) Effect of temperature on the oxidation of benzylamine over CM-773: Reaction conditions: benzylamine (0.2 mmol), time (2 h), catalyst amount (100 mg), and O_2 balloon.

Fig. 6. (A) Effect of reaction time on the oxidation of benzylamine over CM-773: Reaction conditions: benzylamine (0.2 mmol), temperature (393 K), catalyst amount (100 mg), and O_2 balloon. (B) CM-773 catalyst recycling studies: Reaction conditions: benzylamine (0.2 mmol), time (2 h), temperature (393 K), catalyst amount (100 mg), and O_2 balloon.

Scheme 1: A plausible reaction mechanism for oxidative coupling of benzylamine.

Fig. 1

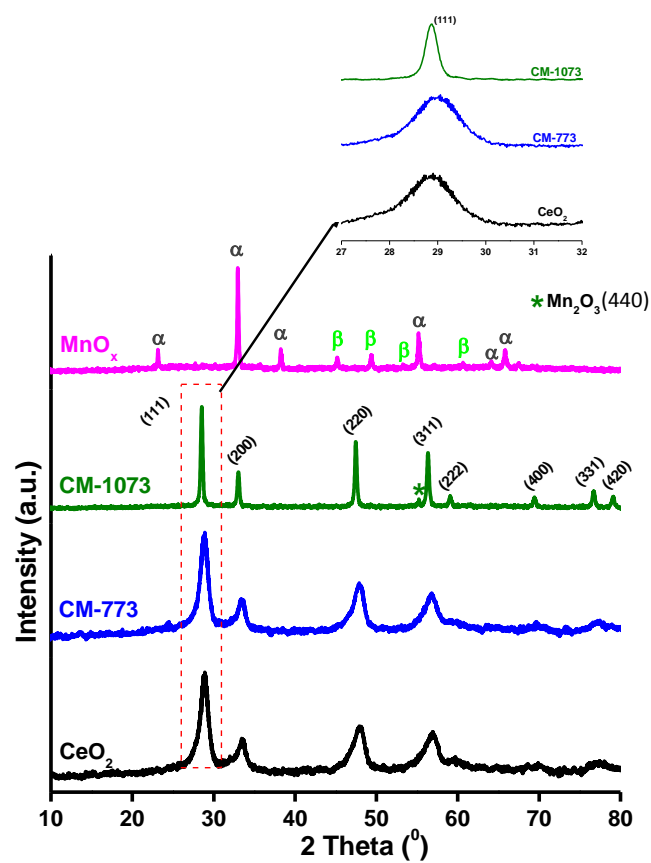


Fig. 2

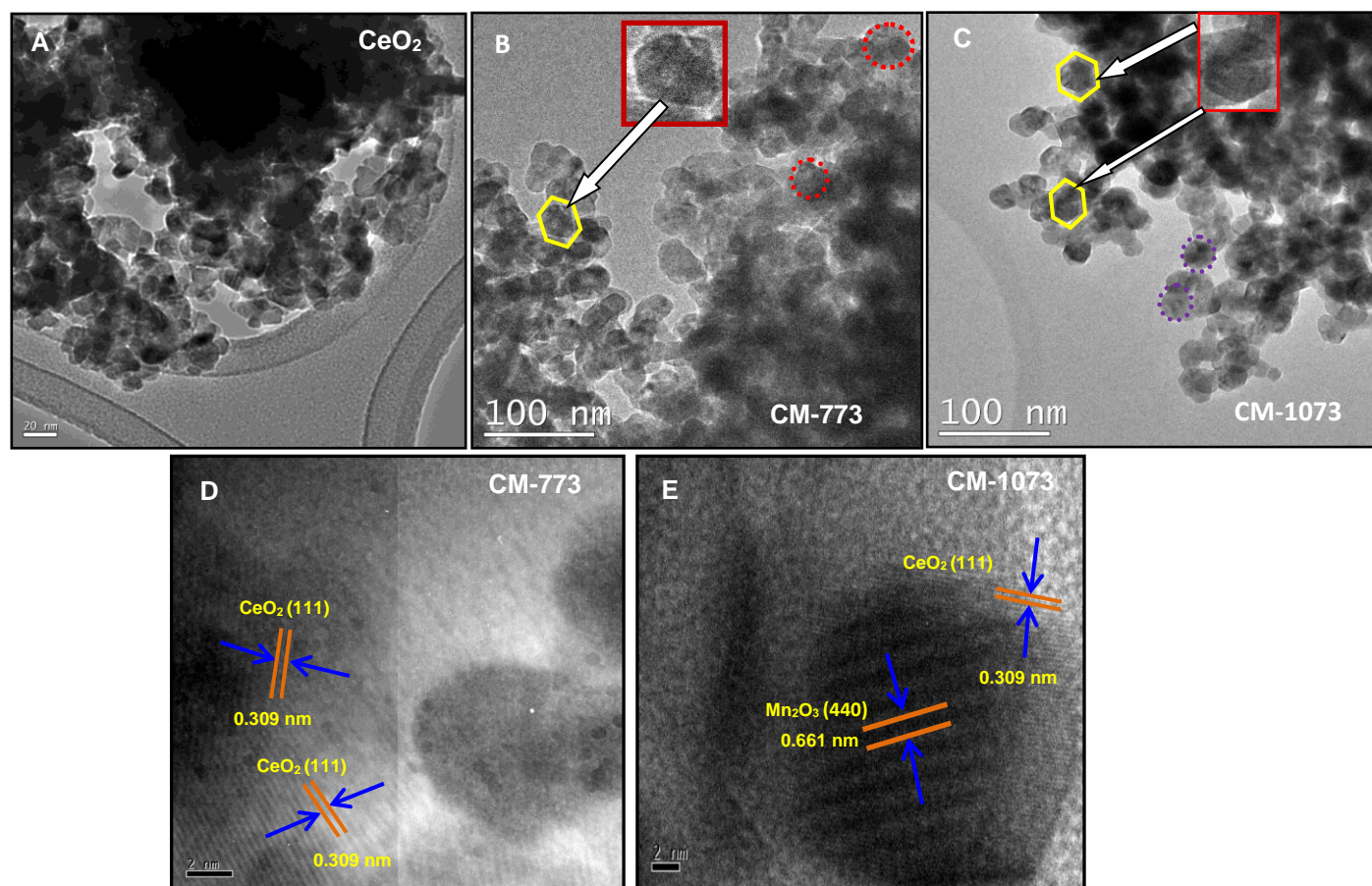


Fig. 3

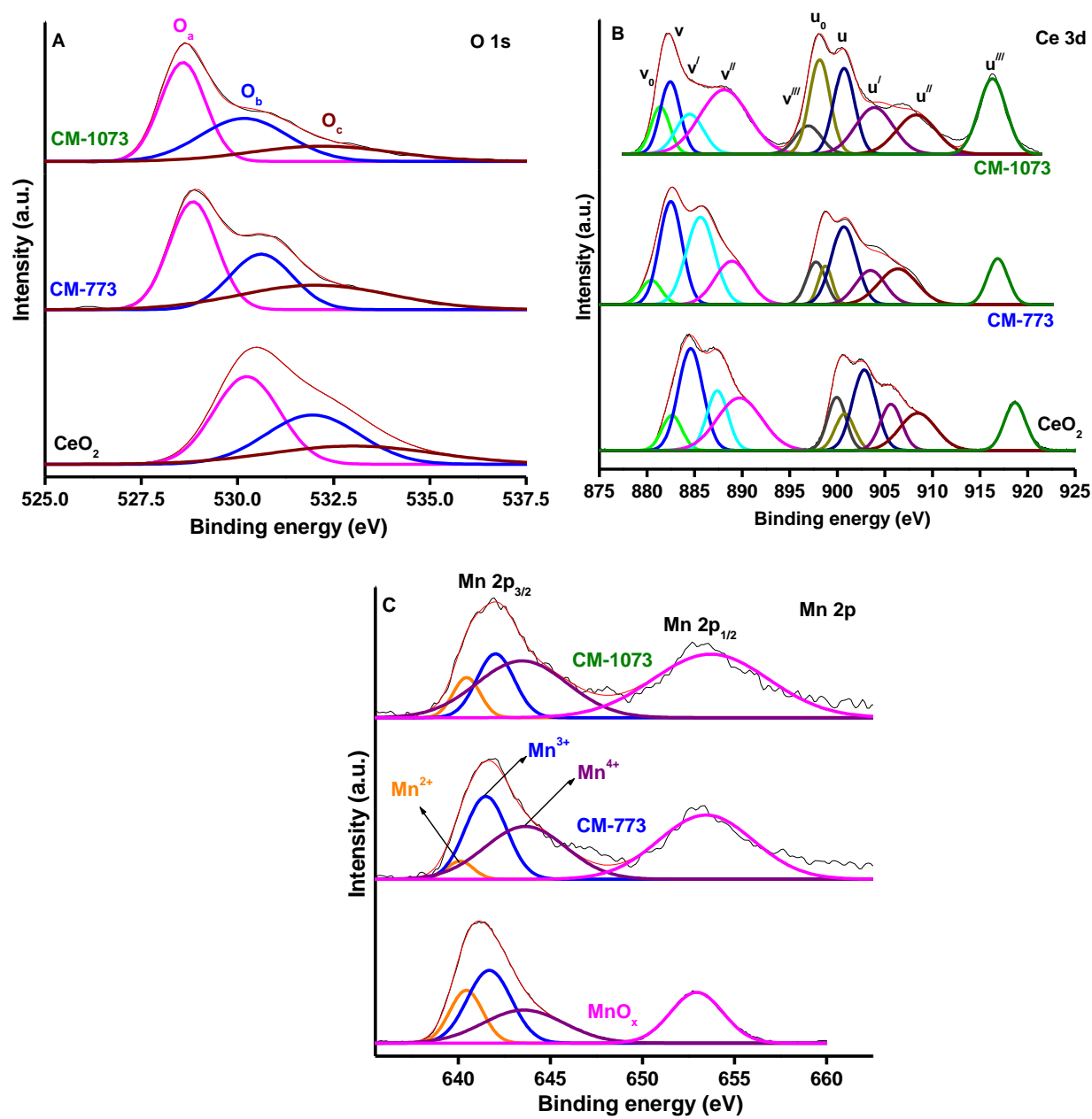


Fig. 4

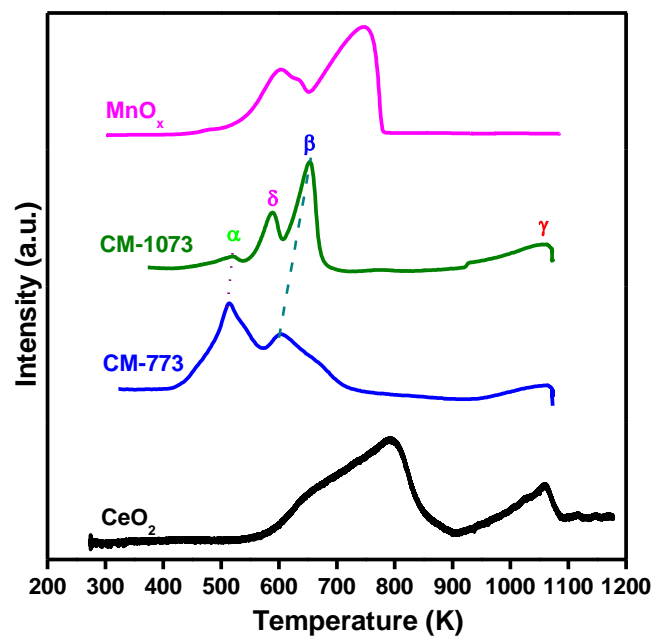


Fig. 5

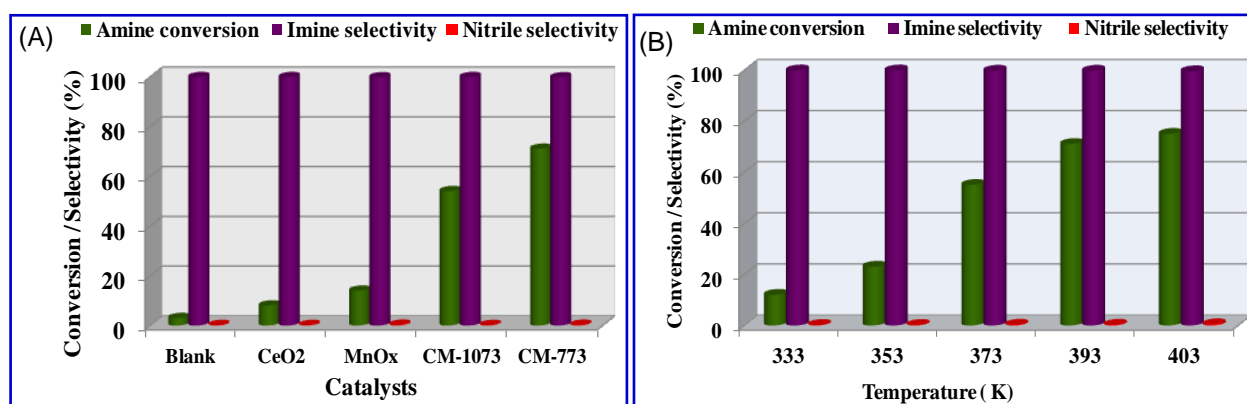
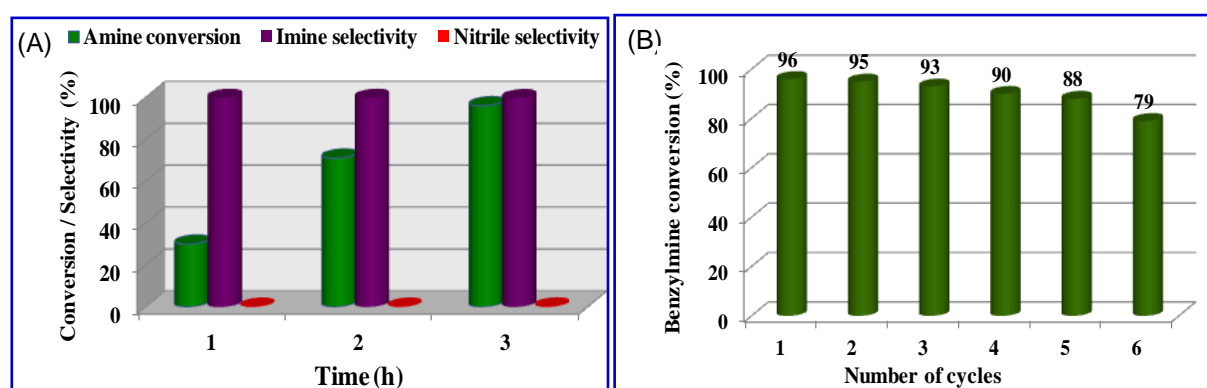


Fig. 6



Scheme 1

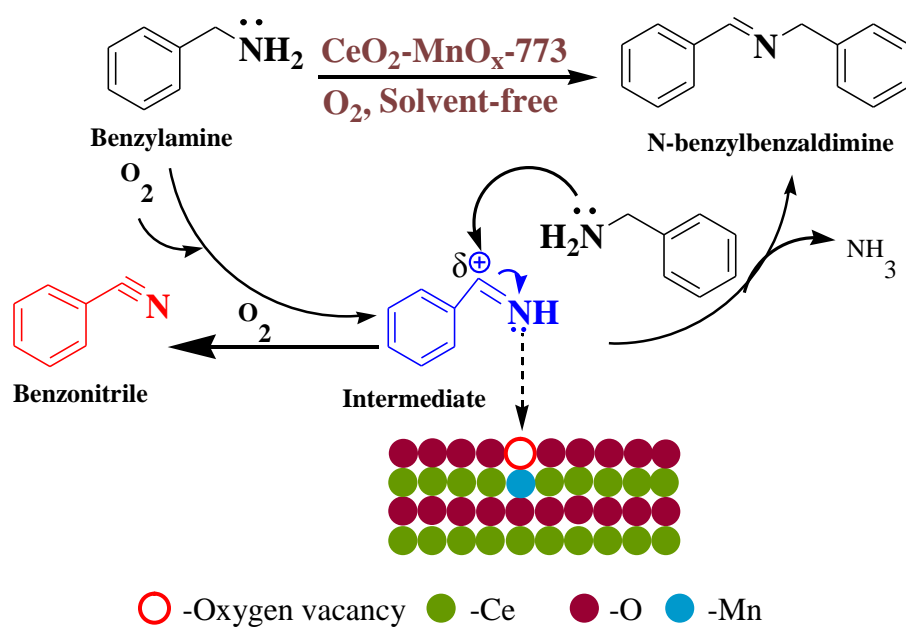


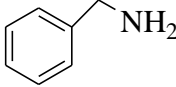
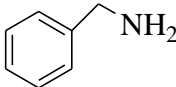
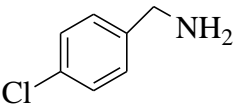
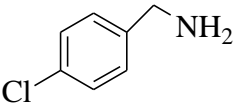
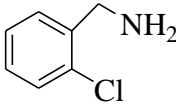
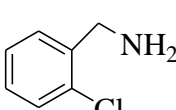
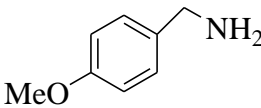
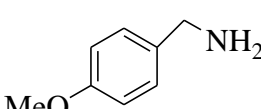
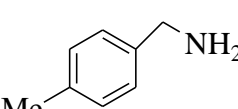
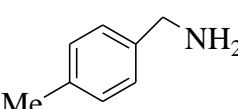
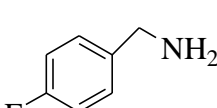
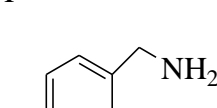
Table 1

BET surface area (SA), average pore size (nm), pore volume (cm^3g^{-1}), average crystallite size (nm), lattice parameter (\AA) of CM samples calcined at different temperatures 773 and 1073 K and pure CeO_2 and MnO_x calcined at 773 K.

Sample	SA	Average pore	Pore volume	D (nm)	LP
	m^2g^{-1}	size (nm)	$(\text{cm}^3\text{g}^{-1})$		(\AA)
MnO_x	28	8.2	0.02	32.4	4.71
CeO_2	41	3.9	0.04	8.92	5.41
CM-773	58	30.1	0.44	7.19	5.35
CM-1073	11	40.6	0.11	22.35	5.41

Table 2

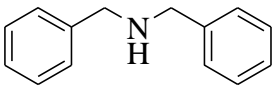
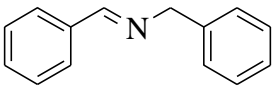
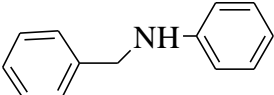
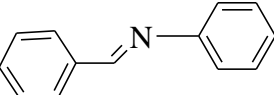
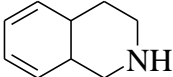
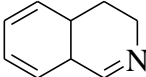
Aerobic oxidative coupling of various substituted benzylamines over CM-773 catalyst under solvent-free conditions.

Serial no	Amine	Time (h)	Conversion (%)	Selectivity (%)	
				Imine	Nitrile
1		2	71	99.8	0.2
2		3	96	99.7	0.3
3		2	76	99.8	0.2
4		3	98	99.6	0.4
5		2	69	99.9	0.1
6		3	89	99.8	0.2
7		2	83	99.7	0.3
8		3	99	99.5	0.5
9		2	79	99.8	0.2
10		3	98	99.7	0.3
11		2	74	99.7	0.3
12		3	94	99.6	0.4

Reaction conditions: temperature (393 K), amine (0.2 mmol), catalyst amount (0.1 g) and oxygen balloon.

Table 3

Oxidation of various secondary benzylamines over CM-773 catalyst.

Serial no	Amine	Conversion (%)	Selectivity (%)
1		78	 (100)
2		64	 (100)
3		60	 (100)

Reaction conditions: temperature (393 K), Time (2h), amine (0.2 mmol), catalyst amount (0.1 g) and oxygen balloon.